Non-cubic distortions in quadratic $E \otimes e$ Jahn-Teller systems

Elie A. Moujaes, Janette L. Dunn,* and Colin A. Bates
School of Physics and Astronomy, University of Nottingham, Nottingham, NG7 2RD, United Kingdom
(Received 16 April 2008; revised manuscript received 10 June 2008; published 12 August 2008)

We investigate the $E \otimes e$ Jahn-Teller (JT) system when both linear and quadratic couplings are included and when it is subjected to external symmetry-lowering distortions. Such distortions could, for example, be due to intrinsic molecular geometry, strains applied to a cubic crystal, and as the result of cooperative interactions between different JT centers. It is well known that the lowest adiabatic potential-energy surface consists of a warped trough containing up to three minima depending on competition between the symmetry-lowering distortion and the quadratic coupling. The motion of the system can be divided into a vibration across the trough and a hindered pseudorotation around the trough. We will construct an analytical form for the wave function involving electronic, vibrational, and pseudorotational contributions that is valid for a wide range of coupling strengths. The wave function is then used to calculate the energy of the ground state of the system. The results are compared to those from a numerical Lanczos diagonalization procedure. We find that in strong linear coupling there tends to be very little dependence on either the strength of the distortion or the value of the quadratic coupling constant. This is not true for weaker linear coupling. We show that much of the behavior of the system can be deduced from analyzing the form of the potential, so that it is not necessary to perform a complete analysis of the wave functions and their energies.

DOI: 10.1103/PhysRevB.78.085412 PACS number(s): 71.70.Ej

I. INTRODUCTION

The electron-phonon interaction in a molecule or a crystal often plays a crucial role in many of the observed phenomena in physics. Of particular importance is the Jahn-Teller (JT) effect,[1] in which the electron-phonon interaction will take a system to a more stable configuration by lowering the symmetry and, hence, the degeneracy of that system. The stable configurations can be associated with minima in the lowest adiabatic potential-energy surface (APES). In fact, quantum tunneling between the minima usually restores the original symmetry in isolated atoms and molecules. This is known as the dynamic JT effect. However, some systems may have a lower symmetry due to other factors. The shape of some molecules may result in a small intrinsic distortion from a higher symmetry. For JT solids, applied or induced strains can produce symmetry-lowering distortions. Interactions between different JT centers in the cooperative JT effect (CJT) (Ref. 2) can also cause a net symmetry lowering. For simplicity in this paper, we will call all external symmetry-lowering distortions "strains," irrespective of the origin of the distortions. This is not restricted to strain in a mechanical sense.

The CJT is believed to affect the electronic properties of materials in a number of different ways. Some compounds undergo a phase transition from an undistorted configuration at high temperatures to a state where distortions are locked in place at low temperatures,[3] causing changes in the shape of the solid in question. This is especially important in materials where the JT distortion is large, such as in the $LaMnO_3$ compounds[4,5] and in spinels.[6] Other examples of much interest, particularly at low temperatures, are the fullerene compounds involving the C_{60} molecule. In the solid state, interactions between different C_{60} molecules can lock distorted centers in place.[7]

In this paper, we will look at the effects of symmetry-lowering distortions in $E \otimes e$ JT systems, in which a twofold-degenerate electronic E state is coupled to a doubly degenerate e vibrational state when both linear and quadratic couplings are taken into account. Physically, the $E \otimes e$ system can represent triangular molecules such as Na_3 (Refs. 8 and 9) or complexes such as $NaCl:Rh^{2+}$ (Ref. 10). $Cu(H_2O)_6^{2+}$ ions in Cu^{2+}-doped $Zn(H_2O)_6(GeF_6)$, Tutton salts $M_2Zn(H_2O)_6(SO_4)_2$ ($M=K^+$, Rb^+, NH_4^+, and Cs^+), and structural analogs can be modeled by an $E \otimes e$ JT system perturbed by orthorhombic strains.[11,12]

The $E \otimes e$ system has been the subject of numerous studies for over 40 years.[13–15] From a theoretical point of view, as well as being an interesting system in its own right, the $E \otimes e$ system is a model system for more complicated JT systems. Some authors start with analytical formalisms[16–21] while others use first-principle numerical or Lanczos diagonalization methods.[12,22] The numerical approaches may provide good quantitative estimates of energies, but analytical approaches provide more insight into the underlying physics by expressing the associated wave functions in a physical form.[23]

In a previous paper,[24] we investigated the case of strain in the $E \otimes e$ system when only linear JT coupling is considered. In this case, the lowest APES is the well-known so-called Mexican hat potential, in which the minimum points form a continuous trough. The motion of the system will consist of vibrations across the trough and pseudorotations around the trough. The addition of a strain then warps the trough so that the pseudorotations become hindered. Due to the symmetry of the Mexican hat, strains in different directions will produce results equivalent to each other. However, when quadratic coupling is included, this is only the case when the strain is sufficiently strong compared to the quadratic coupling that a single point on the trough becomes lowest in energy. In all other cases, there will be a more complicated hindered pseudorotational and vibrational motion.

Quadratic coupling warps the Mexican hat into a tricorn with three equivalent minima [Fig. 1(a)]. Following conven-

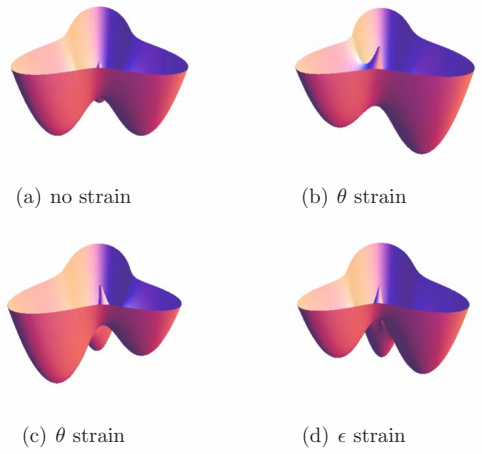

FIG. 1. (Color online) The energy of the lowest APES as a function of Q_θ and Q_ϵ. (a) Three equivalent minima are formed with linear and quadratic couplings. (b) and (c) Addition of a θ-type strain lowers either one or two of the wells (depending on its sign). (d) An ϵ-type strain results in three wells with different energies.

tion, we will label the two components of the e mode θ and ϵ. One of the minima is in the Q_θ direction and the other two are at 120° to the Q_θ direction in the Q_θ-Q_ϵ plane. All directions are no longer equivalent and, away from the strong strain limit, strains in different directions will have different effects. The addition of a strain in the same direction as one of the wells produced by the quadratic coupling, such as a strain in the Q_θ direction, will cause that well to be lower in energy than the other two. This is shown in Fig. 1(b). A strain of the opposite sign will lower the other two wells as shown in Fig. 1(c). For strains in all other combinations of Q_θ and Q_ϵ directions, all equivalences between wells are lost and the strain will result in three wells of different energies as shown in Fig. 1(d). It is therefore necessary to consider all strain directions when considering the effects of both strain and quadratic coupling. While this makes the mathematics of the problem considerably more complicated, it also introduces a different physics compared to the situation where the strain is in the same direction as one of the wells.

Traditionally, quadratic coupling has been considered to be the dominant mechanism for warping the trough in the APES in the $E \otimes e$ problem. However, anharmonic terms (cubic in the Q's), pseudo-JT effects, and other higher-order interactions can also produce warping. In fact, there have been recent suggestions that cubic anharmonic terms could cause the largest contribution to the potential barriers between wells in $NaCl:Rh^{2+}$ and triangular molecules such as Ag_3,[10] although other later calculations have found little influence from the cubic contributions for Ag_3.[25] However, these warping mechanisms will still result in three wells with the only difference being in the shape of the potential surface away from the minima. Thus our results provide a good indication of the behavior with these other couplings also.

In this paper, we will show how an analytical form for the wave function of any $E \otimes e$ system with linear, quadratic, and non-cubic "strain" terms can be constructed. It follows on from previous work in the strong JT coupling limit[6] and extends our previous work that did not include quadratic couplings.[24] The wave function contains contributions from the electronic motion, vibrational motion across wells, and motion that represents either a vibration or a hindered pseudorotation in the direction of the trough in the Mexican hat potential, depending on the strength of the different contributions to the potential. We will then explore the potential and wave function—illustrating how the competition between quadratic coupling and strain is evident for some parameter ranges, while for other ranges there is much less of an effect. We will calculate the energy of the ground state of the system using our wave function and show how much of the dependence of the energy on the linear, quadratic, and warping parameters could be deduced from a simple analysis of the potential. The values for the energies will also be compared to those obtained by solving the problem numerically using a Lanczos diagonalization technique.

II. HAMILTONIAN

Since the $E \otimes e$ JT problem involves two components (θ and ϵ) of the vibrational e mode, the general Hamiltonian for the quadratic system with strain should contain strain terms in these two directions. The Hamiltonian describing a specific molecule in an electronic basis $(\phi_\theta, \phi_\epsilon)$ is thus

$$\mathcal{H} = \mathcal{H}_{\text{vib}} + \mathcal{H}_{\text{int}} + W_E[(Q_\theta^2 - Q_\epsilon^2)\sigma_\theta - 2Q_\theta Q_\epsilon \sigma_\epsilon] - w_\theta \sigma_\theta - w_\epsilon \sigma_\epsilon, \tag{1}$$

where

$$\mathcal{H}_{\text{vib}} = \frac{1}{2\mu}(P_\theta^2 + P_\epsilon^2) + \frac{\mu \omega_E^2}{2}(Q_\theta^2 + Q_\epsilon^2),$$

$$\mathcal{H}_{\text{int}} = V_E(Q_\theta \sigma_\theta + Q_\epsilon \sigma_\epsilon). \tag{2}$$

V_E and W_E are the linear and quadratic coupling constants, respectively, and w_θ and w_ϵ are the strains in the θ and ϵ directions of coordinate space, respectively. Q_ν and P_ν are, respectively, the collective coordinates and corresponding momenta for an intramolecular vibrational mode $\nu = (\theta, \epsilon)$. w_E is the frequency of the modes and μ is the reduced mass of the system. σ_θ and σ_ϵ are 2×2 matrices of Clebsch-Gordon coefficients given by $\sigma_\theta = \sigma_z/2$ and $\sigma_\epsilon = -\sigma_x/2$, where

$$\sigma_z = \begin{pmatrix} 1 & 0 \\ 0 & -1 \end{pmatrix}, \quad \sigma_x = \begin{pmatrix} 0 & 1 \\ 1 & 0 \end{pmatrix}. \tag{3}$$

This is an equivalent Hamiltonian to that used in Refs. 10 and 12 except that they include an additional anharmonic term and the former defines their Q_ϵ to have opposite sign to ours.

The Hamiltonian can be converted into a more convenient form by adopting the set of transformations used by Sato *et al.*[21] This involves converting to the complex two-dimensional electronic basis (ψ_+, ψ_-), which is related to the usual electronic basis $(\phi_\theta, \phi_\epsilon)$ by

$$\psi_+ = \frac{1}{\sqrt{2}}(\phi_\theta + i\phi_\epsilon),$$

$$\psi_- = \frac{1}{\sqrt{2}}(\phi_\theta - i\phi_\epsilon). \tag{4}$$

Transforming to polar coordinates involving the radial and angular coordinates ρ and ϕ, respectively, where $\{Q_\theta, Q_\epsilon\} = \rho\{\cos\phi, \sin\phi\}$ and noting that $P_\nu = -i\hbar\partial/\partial Q_\nu$, the Hamiltonian in matrix form is

$$\mathcal{H} = \left[-\frac{\hbar^2}{2\mu}\frac{\partial^2}{\partial\rho^2} + \frac{\mu\omega_E^2}{2}\rho^2 - \frac{\hbar^2}{8\mu\rho^2}\right]\sigma_0 + \frac{\hat{L}_z^2}{2\mu\rho^2} - \frac{w_\theta}{2}\sigma_x - \frac{w_\epsilon}{2}\sigma_y + \frac{V_E}{2}\rho\begin{pmatrix} 0 & e^{-i\phi} \\ e^{i\phi} & 0 \end{pmatrix} + \frac{W_E}{2}\rho^2\begin{pmatrix} 0 & e^{2i\phi} \\ e^{-2i\phi} & 0 \end{pmatrix}, \tag{5}$$

where

$$\sigma_0 = \begin{pmatrix} 1 & 0 \\ 0 & 1 \end{pmatrix}, \quad \sigma_y = \begin{pmatrix} 0 & -i \\ i & 0 \end{pmatrix}, \tag{6}$$

and $\hat{L}_z$ is the z component of the angular-momentum operator. One further transformation of the form

$$S = \frac{1}{\sqrt{2}}\begin{pmatrix} e^{-i\phi/2} & e^{-i\phi/2} \\ e^{i\phi/2} & -e^{i\phi/2} \end{pmatrix} \tag{7}$$

will transform the overall Hamiltonian into

$$\mathcal{H} = \left[-\frac{\hbar^2}{2\mu}\frac{\partial^2}{\partial\rho^2} + \frac{\mu\omega_E^2}{2}\rho^2 - \frac{\hbar^2}{8\mu\rho^2}\right]\sigma_0 + \frac{1}{2\mu\rho^2}\left(\hat{L}_z - \frac{1}{2}\sigma_x\right)^2 + \frac{V_E}{2}\rho\sigma_z - \frac{w_\theta}{2}(\cos\phi\sigma_z + \sin\phi\sigma_y) - \frac{w_\epsilon}{2}(\sin\phi\sigma_z - \cos\phi\sigma_y) + \frac{W_E}{2}\rho^2(\cos 3\phi\sigma_z + \sin 3\phi\sigma_y). \tag{8}$$

This is the same equation as in Sato *et al.*'s Eq. (7) with their linear coupling constant $g = V_E/2$ and with the addition of quadratic coupling and strain terms.

The terms in σ_x and σ_y are off diagonal, which causes mixing between the different APESs. These represent a higher-order correction and therefore will be dropped. The matrix form of the Hamiltonian in Eq. (8) then contains two differential equations, which describe the motion on the lower and upper APESs. As we are interested in the low-lying states, which reside on the lowest APES, we only need to study the equation

$$\mathcal{H} = -\frac{\hbar^2}{2\mu}\frac{\partial^2}{\partial\rho^2} + \frac{1}{2\mu\rho^2}\hat{L}_z^2 + U_{\text{eff}}(\rho,\phi), \tag{9}$$

where

$$U_{\text{eff}}(\rho,\phi) = \frac{1}{2}(\mu\omega_E^2\rho^2 - V_E\rho + w_\theta\cos\phi + w_\epsilon\sin\phi - W_E\rho^2\cos 3\phi). \tag{10}$$

U_{eff} is the potential used to illustrate the shape of the APES in Fig. 1. When the ϵ-type terms are set to zero ($w_\epsilon = 0$), the ϕ dependence of Eq. (9) is equivalent to Eq. (10) of Ref. 6 and the additional potential terms are the same as in Eq. (2) of Ref. 26.

III. DETERMINATION OF THE WAVE FUNCTIONS

In order to find suitable solutions to Eq. (9), it is instructive to examine the form of the lowest APES, defined by U_{eff}, and the resulting motion that is likely to arise. We have already noted that in the general case of the quadratic $E\otimes e$ system with strain, there are three nonequivalent minima in the APES [Fig. 1(d)]. The positions of the lowest-energy point depend on a competition between the strain and quadratic coupling terms. In strong strain, the equilibrium position can occur at a very different position from the positions of any of the three minima in the absence of any strain. This will be discussed again in more detail in Sec. VI.

Assuming that the barriers between the wells due to the quadratic coupling and strain terms are such that we have a hindered rotation around the trough and vibrations across it, the total wave function $\Psi(\rho,\phi)$ comprises electronic, vibrational, and pseudorotational components. As Eq. (9) represents coupled equations, it is not possible to write down separate expressions for the different components of the motion without any approximations. We therefore note that when strain is added to the linear coupling problem, the distance of the minimum-energy point from the origin is, to a first approximation, the same as the radius of the trough in linear coupling only.[24] If we assume that the radius of the minimum-energy point is unaltered by strain, it is possible to treat the value of ρ in the part of the equations describing the motion around the trough as a constant. This allows us to separate the variables in the differential equation in ρ and ϕ. We will therefore make the same assumption here when strain is added to a system with linear and quadratic couplings. This means that minimum positions (or wells) in the APES will occur at a radius

$$\rho_E = \frac{V_E}{2\mu\omega_E^2(1 - W_E')}, \tag{11}$$

where $W_E' = W_E/\mu\omega_E^2$ is a dimensionless version of the quadratic coupling constant W_E.

The energy of the lowest points on the trough of the undistorted system with linear and quadratic couplings is called $-E_{JT}$, where E_{JT} is the JT energy. With the above assumption concerning separation into radial and transverse motion, E_{JT} can be determined by substituting $\rho = \rho_E$ and $\phi = 0$ into Eq. (10), giving

$$E_{JT} = \frac{V_E^2}{8\mu\omega_E^2(1 - W_E')}. \tag{12}$$

Also, we will denote the electronic, vibrational, and rotational components of the total wave function by $\psi(\phi)$, $\chi(\rho_E)$,

and $\Phi(\phi)$, respectively. Thus, with this assumption, $\Psi(\rho,\phi)$ can be written in the form

$$\Psi(\rho,\phi) = \psi(\phi)\chi(\rho_E)\Phi(\phi). \tag{13}$$

The electronic part of the wave function in the (ψ_+,ψ_-) basis has the form[24]

$$\psi(\phi) = -\frac{1}{\sqrt{2}}\begin{pmatrix} e^{-i\phi/2} \\ -e^{-i\phi/2} \end{pmatrix}. \tag{14}$$

The vibrational part is governed by the classical harmonic-oscillator differential equation

$$-\frac{\hbar^2}{2\mu}\frac{d^2\chi(\rho)}{d\rho^2} + \frac{\mu\omega_E^2}{2}\rho^2\chi(\rho) = E_{\text{vib}}\chi(\rho) \tag{15}$$

and, with the assumption that we can write $\rho=\rho_E$ for the rotational motion, the rotational equation becomes

$$-\frac{\hbar^2}{2\rho_E^2}\frac{d^2\Phi(\phi)}{d\phi^2} + \frac{1}{2}(w_\theta \cos\phi + w_\epsilon \sin\phi)\Phi(\phi) - \frac{W_E}{2}\rho_E^2 \cos 3\phi\, \Phi(\phi) = E_\phi \Phi(\phi). \tag{16}$$

Equation (15) for the vibrational equation has well-known solutions. However, Eq. (16) for the rotational motion cannot be solved analytically as it stands. However, it is possible to find a series solution in $\cos\frac{\phi}{2}$ and $\sin\frac{\phi}{2}$. Since the total wave function is invariant under the transformation $\phi\rightarrow\phi+2\pi$ and the electronic wave function changes sign, the rotational part must be antiperiodic. This means that the series solution must only involve odd powers, which leads to a solution of the form

$$\Phi(\phi) = \sum_{n=0}^{\infty}\left[A_{2n+1}\cos^{2n+1}\left(\frac{\phi}{2}\right) + B_{2n+1}\sin^{2n+1}\left(\frac{\phi}{2}\right)\right]. \tag{17}$$

For θ-type strains only, this is consistent with Ref. 6 which carried out a numerical matrix diagonalization using basis states involving $\cos[(2m-1)\phi/2]$ and $\sin[(2m-1)\phi/2]$ $(m=1,2\ldots)$.

Obviously it is not possible to continue the sum to infinity; therefore, it will be truncated at $n=18$. This leads to a sequence of wave functions with corresponding rotational energies E_ϕ.

The total energy is

$$E_e = \frac{\int_0^{2\pi}\int_0^{2\pi}\Psi(\rho_E,\phi')\mathcal{H}\Psi(\rho_E,\phi)d\phi d\phi'}{\int_0^{2\pi}\int_0^{2\pi}\Psi(\rho_E,\phi')\Psi(\rho_E,\phi)d\phi d\phi'}, \tag{18}$$

and it depends on V_E, W_E, w_θ, and w_ϵ. Note that the effects of quadratic coupling and strain are built into the rotational wave function as it depends on the values of W_E, w_θ, and w_ϵ.

As can be seen from Eq. (18) the formalism we use for calculating the energy involves an integration using a wave function that incorporates electronic, vibrational, and rotational effects. This can be expected to give good results for all strong and intermediate coupling strengths. It is different to that used by Englman and Halperin[6] who separately determine the energy of the vibrational motion across the trough and then incorporate that energy as a constant (i.e., a term independent of ϕ) into a differential equation in ϕ. This is only valid for the limit of strong linear coupling.

IV. RESULTS

We will start by examining the lowest-energy rotational wave function $\Phi(\phi)$ and its relation to the effective potential U_{eff} in Eq. (10) for fixed values of the dimensionless linear coupling constant $V'_E=V_E/\sqrt{\hbar\mu\omega_E^3}$, the dimensionless quadratic coupling constant W'_E, and for different values of the dimensionless distortion parameters $w'_\theta=w_\theta/\hbar\omega_E$ and $w'_\epsilon=w_\epsilon/\hbar\omega_E$. We can choose any 2π range of ϕ to specify the positions of these minima. We will choose a range from $-\pi$ to π. When there is no strain, quadratic coupling then results in three equivalent minima in the APES at positions given by $\phi=0$, $-2\pi/3$, and $2\pi/3$. If the range from 0 to 2π is chosen, then there will be a minimum at the end point of the range, which will make plots of the APES as a function of ϕ more difficult to visualize.

We will consider first the effective potential when $w'_\epsilon=0$. In the absence of any quadratic coupling, where there is a trough of minimum-energy points with no strain, the point on the trough at $\phi=\pi$ will be pushed lowest in energy when w'_θ is positive and the point at $\phi=0$ lowest in energy when w'_θ is negative. Therefore, when quadratic coupling is included, the situation with a negative coefficient w'_θ is clear; both the quadratic coupling and strain enhance a minimum at $\phi=0$. This point therefore becomes an absolute minimum. There are still minima near $-2\pi/3$ and $2\pi/3$, but these are local minima corresponding to a larger value of energy. This is shown in Fig. 2(a) for $w'_\theta=-0.2$ (and $w'_\epsilon=0$) with a value of linear coupling $V'_E=2$ and a value of quadratic coupling $W'_E=0.1$.

When the coefficient w'_θ is positive, there is a competition between the quadratic coupling and the strain. When the quadratic coupling is sufficiently strong compared to the strain to still have a strong effect, there will be two equivalent global minima near $-2\pi/3$ and $2\pi/3$. In this case, the minima at $\phi=0$ are now only a local minimum. This is shown in Fig. 2(b) for $w'_\theta=0.2$, $w'_\epsilon=0$, $V'_E=2$, and $W'_E=0.1$ as before. There is also a displacement of the positions of the minimum at $-2\pi/3$ toward $-\pi$ and an equivalent displacement of the minimum at $2\pi/3$ toward π. In fact, when $w'_\epsilon=0$, it follows from Eq. (10) that turning points in the APES are at $\sin\phi=0$ and positions ϕ satisfying the equation

$$\cos^2\phi = \frac{w_\theta + 3W_E\rho^2}{12W_E\rho^2}. \tag{19}$$

This shows that the displacement of the minima toward $\pm\pi$ will increase as the strength of the strain w_θ increases compared to the product of the quadratic coupling W_E and ρ^2

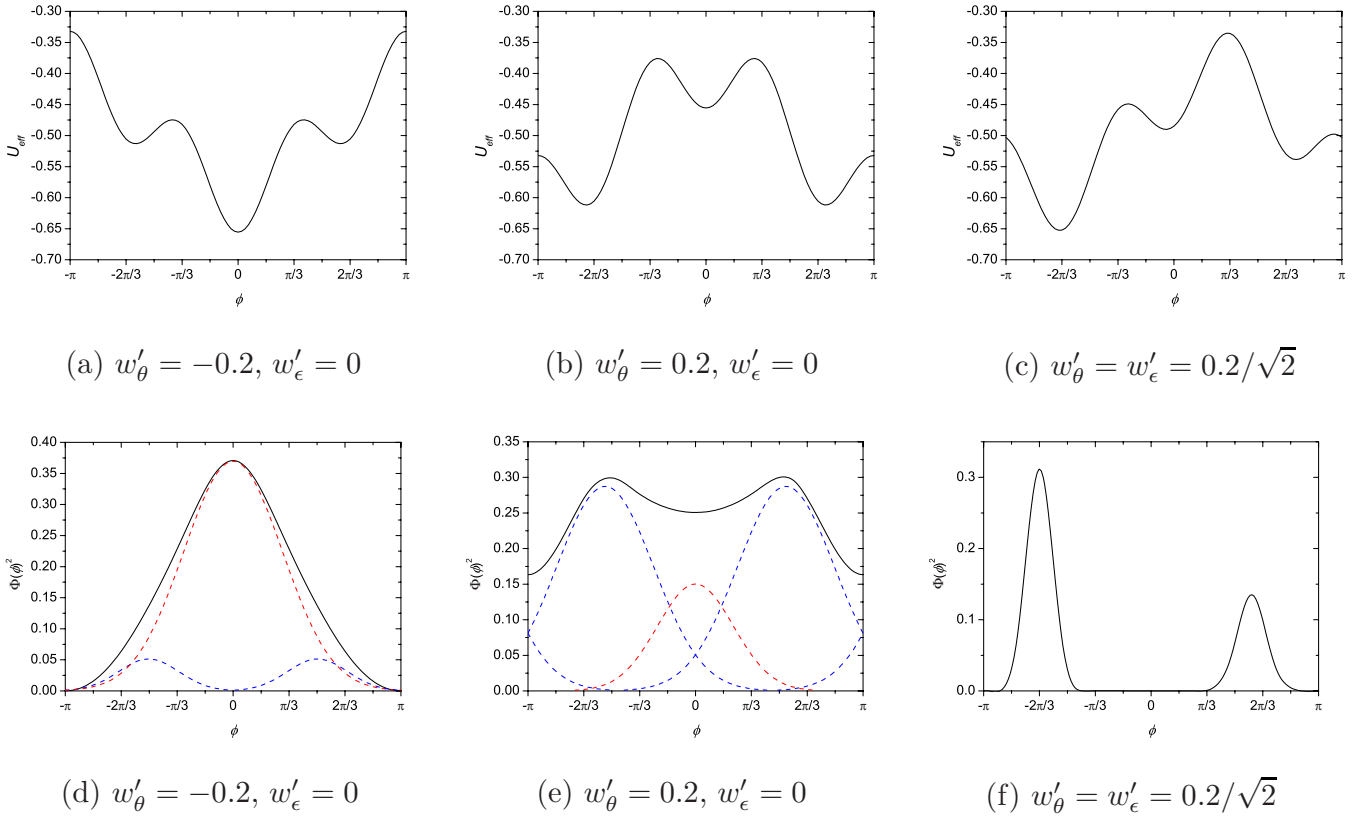

FIG. 2. (Color online) (a)–(c) Show the effective potential as a function of the angle ϕ at radius ρ_E for three different values of the strains w'_θ and w'_ϵ. All of the plots are for V'_E=2 and W'_E=0.1. (d)–(f) show the square of the rotational wave function $\Phi(\phi)$ for the same three strains. (d) and (e) also show a fit of $\Phi(\phi)^2$ to three Gaussians, allowing for a periodicity of 2π in ϕ.

until above $w_\theta = 9W_E\rho^2$, where there it becomes a single minimum at $\pm\pi$.

The strain with coefficient w'_ϵ is in the Q_ϵ direction. Quadratic coupling does not produce wells in this direction, and there is no symmetry in the positions of the wells with respect to this direction. When combined with quadratic coupling, we will therefore have three nonequivalent local minima. Figure 2(c) shows the result for the case $w'_\theta = w'_\epsilon = 0.2/\sqrt{2}$. In this example, the minimum near $-2\pi/3$ is the global minima and the minima near 0 and $2\pi/3$ are local minima.

We will now examine the rotational wave function $\Phi(\phi)$ in relation to U_{eff}. It can be expected that the system is most likely to be found in a distorted configuration corresponding to the angles ϕ that give minima in the APES. This means that plots of $\Phi(\phi)^2$ should have maxima close to these positions. Figures 2(d)–2(f) show $\Phi(\phi)^2$ for the same parameters used to plot U_{eff} in Figs. 2(a)–2(c), respectively. Figure 2(d) exhibits one peak at ϕ=0 while Fig. 2(e) exhibits two peaks close to $\pm 2\pi/3$. The positions of these peaks are close to the global minima in the APES for these parameters, as is to be expected. In the case of Fig. 2(e), the largest peak is near $-2\pi/3$, which corresponds to the global minimum in the APES, but there is also a subsidiary peak near $+2\pi/3$. This corresponds to a local minimum in the APES and indicates that, while there is no global minimum at this value, there is still a small probability of finding the system in this configuration.

Reference 26 obtained plots for the potential at fixed radius for θ-type distortions only when considering Cu^{2+} ions in K_2ZnF_4, which shows that either one well or two wells are lowest with this particular strain direction depending on the sign of the strain term. Similar features were noted in Ref. 6 for this type of strain. Reference 12 obtained plots for the potential at fixed radius for specific parameter values relevant to $Zn(H_2O)_6(GeF_6)$ and the Tutton salts. Their potentials also show a competition between minima and our results are consistent with theirs. Reference 12 also gives schematic representations of the vibronic wave functions. These schematic sketches agree with our quantitative results.

We can further analyze the shape of $\Phi(\phi)^2$ by fitting the results to three Gaussians. It is also necessary to build in periodicity of 2π by translating values less than $-\pi$ by $+2\pi$ and values more than $+\pi$ by -2π. In all three cases, the results fit three Gaussians centered near ϕ=0 and $\phi = \pm 2\pi/3$ almost exactly. The results are shown as dashed lines in Figs. 2(d) and 2(e). For Fig. 2(f), there is a Gaussian centered near ϕ=0 but it is too small to be observable in the figure. The two peaks are themselves almost exact Gaussians, so there are no additional curves to be displayed. The results of the Gaussian fits indicate that, in all cases, there are contributions to the wave function from all local minima in the APES even if this is not obvious at first sight from the shape of $\Phi(\phi)^2$.

As the driving feature of the above plots is a competition between strain and quadratic coupling, it is useful to rep-

arametrize the strains w'_θ and w'_ϵ in polar form

$$w'_\theta = w_0 \cos \alpha,$$

$$w'_\epsilon = w_0 \sin \alpha, \tag{20}$$

where w_0 represents the magnitude of the total strain and α represents its direction (in coordinate space). We can then investigate variations in both the minimum in U_{eff} and in the total energy of the system as a function of the strain angle α for a fixed strain magnitude w_0 (and fixed linear and quadratic couplings). The three cases considered in Fig. 2 correspond to $w_0=0.2$ and $\alpha=\pi$, 0, and $\pi/4$, respectively.

We have already seen that the minimum in U_{eff} at $\phi=0$ is enhanced by a negative θ-type strain, which corresponds to $\alpha=\pi$. Similarly, the minimum at $\phi=2\pi/3$ is enhanced by a strain with $\alpha=5\pi/3$ and the minimum at $\phi=-2\pi/3$ is enhanced by a strain with $\alpha=\pi/3$. The complete variation of the minimum in U_{eff} with angle is shown in Fig. 3(a) for $V'_E=2$ and $W'_E=0.1$ for the cases $w_0=0.2$ and $w_0=4$. Although the actual values of the minima in U_{eff} depend on w_0, both cases exhibit the threefold periodicity expected from our interpretation of three equivalent wells. The same is true for other values of the coupling constants. As the value of the linear coupling V_E increases, the values of the minimum in U_{eff} become more negative and the variation in the values becomes smaller. For $V'_E=10$ and $W'_E=0.1$, the variation in the value of the minimum in the potential is less than 0.4%. Nevertheless, the pattern of the variation remains the same.

We will now calculate the energy of the lowest rotational state associated with the ground vibronic state (zero-phonon excitations). Figure 3(b) shows $E_e/\hbar\omega_E$ versus the angle α for $w_0=0.1$, $V'_E=2$, and $W'_E=0.1$ as previously. The variation in the total energy exhibits a similar behavior to the variation in the potential U_{eff}. This is to be expected. It means that it is possible to determine much of the behavior of the system simply by examining U_{eff}, which is considerably simpler than determining the total energy of the system.

We will now investigate the dependence of the results for various cases with $w'_\epsilon=0$ on linear coupling V'_E by plotting the variation of the energy as a function of V'_E for various combinations of quadratic coupling and strain. If we plot the energies themselves, the results are dominated by the V_E^2 dependence of E_{JT}. It is therefore more instructive to show the energies relative to an energy E' given by

$$E' = -E_{\text{JT}} - \frac{w_\theta}{2}, \tag{21}$$

which is the energy of the lowest point on the APES when $w'_\epsilon=0$ as given by Eq. (10). We will also compare the results with those obtained numerically using a Lanczos diagonalization method. Lanczos methods are commonly used to solve JT problems and, especially, for finding minimum eigenvalues corresponding to the ground state.[12,26–30] Care must be taken because rounding errors mean that simple Lanczos algorithms may give erroneous results due to a lack of orthogonality.[31] The error can be removed by performing a reorthogonalization of the Lanczos vectors at each recursion but at the expense of a huge increase in computing time.

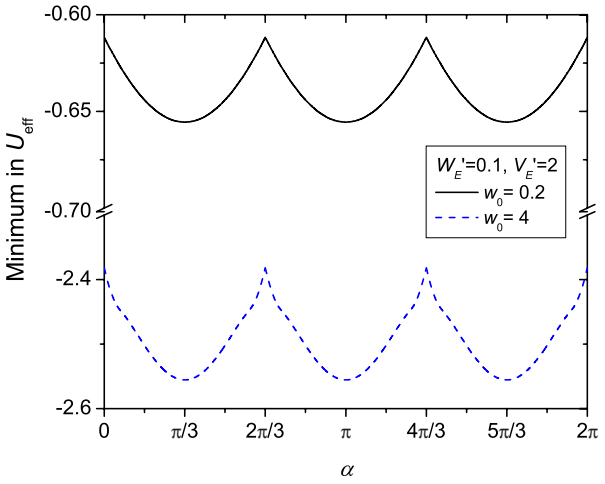

(a) Effective potential

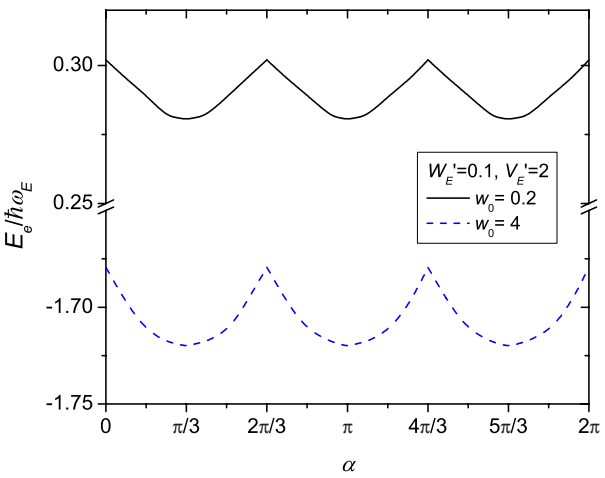

(b) Total energy

FIG. 3. (Color online) (a) Variation of the minimum in U_{eff} as a function of the strain angle α. The magnitude of the total strain w_0 is taken to be 0.2 (solid line) and 4 (dashed line). The linear coupling is $V'_E=2$ and the quadratic coupling is $W'_E=0.1$ in both cases. (b) As for (a) but for the variation in the total energy $E_e/\hbar\omega_E$.

However, good results can be obtained using a selective reorthogonalization block Lanczos method. We have obtained results using the Lanczos selective orthogonalization (LASO) implementation which is a set of FORTRAN IV subroutines for computing a few eigenvalues of a large (sparse) symmetric matrix.[32] We have previously shown that there is good agreement between the results of this method and analytical results for the linear $E\otimes e$ system.[33]

Figure 4 shows curves for the cases where $w'_\theta=0.01$, 1, and 4 with $w'_\epsilon=0$ and $W'_E=0.1$. The continuous lines show the results using our analytical expression for the wave function and the squares show the results from the Lanczos diagonalization. Note that, in all cases, all graphs start from 1 at $V'_E=0$, which is the correct value for a two-dimensional

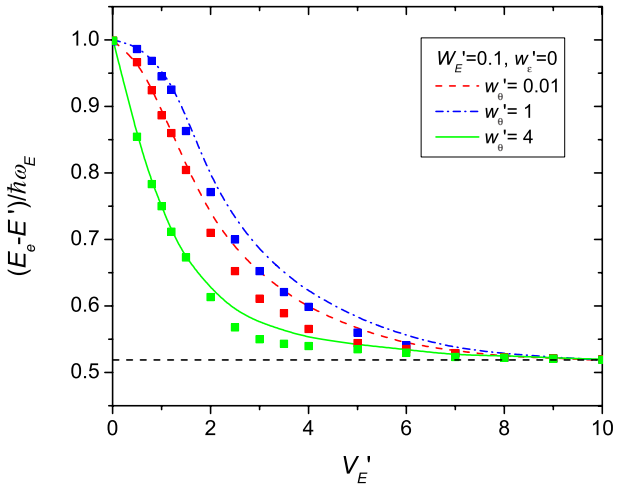

FIG. 4. (Color online) Plots of $(E_e-E')/\hbar\omega_E$ versus V_E' for $W_E'=0.1$ and different combinations of weak and strong strain for the lowest ground rotational state associated with the ground vibronic level. The continuous lines are the results of the analytical calculation and the squares are results from a selective Lanczos orthogonalization method. All cases tend asymptotically to a single value at large V_E' indicated by the dashed horizontal line.

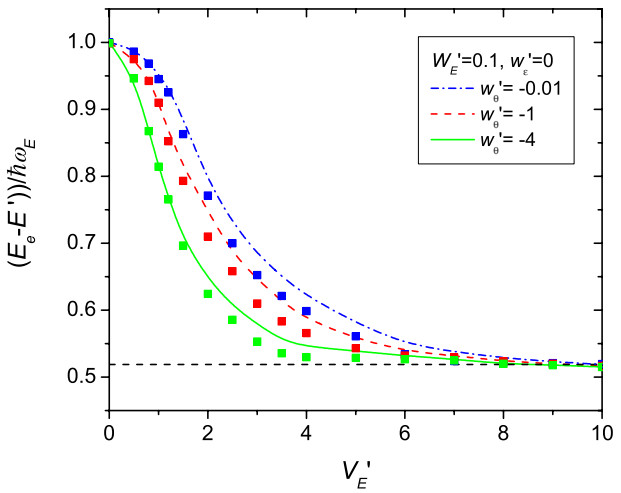

FIG. 5. (Color online) As Fig. 4 but for negative values of w_θ'.

harmonic oscillator with no JT effect. As V_E' increases, we note that in the weak-coupling region smaller values are obtained for larger values of strain. As we move to the strong V_E' regime, we find that the points all tend to the same value (of around 0.519); the results for larger values of linear coupling V_E' result in less sensitivity to strain.

From the form of the effective potential U_{eff} in Eq. (10), we can see that the strength of the quadratic coupling is characterized by the factor $W_E\rho_E^2$ while the strength of the strain is characterized by w_θ and w_ϵ. Also, Eq. (11) shows that the radius of the trough ρ_E is proportional to the linear coupling V_E'. Therefore, as the value of V_E' increases, the effect of the quadratic coupling becomes more dominant over the effect of the strain until the strain has negligible effect. By $V_E'\approx 10$, there is no observable difference in the results for different values of strain with either the analytical or Lanczos results.

It can be seen that the agreement between the analytical and numerical results is excellent in strong and weak coupling. For intermediate couplings, the numerical results for the energy differences $(E_e-E')/\hbar\omega_E$ are slightly smaller than with the analytical method. It has previously been shown that for the linear $E\otimes e$ system, a discrepancy between analytical and numerical results of a similar order of magnitude in intermediate coupling can be attributed to neglect of coupling to the upper APES in the analytical method.[20] Reference 12 also discusses the validity of neglecting coupling to the upper sheet. The same will be true for our results here, as coupling to the upper APES was neglected in going from Eq. (8) to Eq. (9). The coupling to the upper APES could be incorporated into our model. However, the model then becomes considerably more complicated and the advantage of having an analytical model, in which the dependence on the model parameters is clear, becomes lost. We therefore do not attempt this here.

We have also investigated the variation of $(E_e-E')/\hbar\omega_E$ with V_E' for negative values of w_θ' with $w_\epsilon'=0$. Figure 5 shows the cases of $w_\theta'=-0.01$, -1, and -4 with W_E' set to 0.1 as before. Again, the effect of the strain is to reduce the energy in the weak-to-intermediate regime. As we move toward the strong-coupling regime, all the curves tend asymptotically to the same value as with positive strains. This is again because strain has negligible effect in the strong-coupling limit. Also, the differences between the analytical and numerical results are very similar to that for the positive strains.

If similar plots to those in Figs. 4 and 5 are made but for a larger value of quadratic coupling (such as $W_E'=0.6$), then we find that all of the results are almost independent of the strain values chosen. This is consistent with our interpretation that as long as the quadratic coupling is strong enough to generate three deep wells, the addition of an extra strain will have a negligible effect. Furthermore, curves for different values of quadratic coupling when the θ-type strain w_θ is fixed to be a large positive constant do not show any significant differences between each other. This includes the case of zero quadratic coupling. This is because the large strain has generated a single deep well at the same position as one of the three wells that are generated by quadratic coupling, so adding quadratic coupling has no additional effect in this case. The same argument holds when a strain is applied in the same direction as either of the other wells.

We have restricted our observations to the ground vibronic and rotational states. Similar conclusions also apply to the higher excited states. For example, the results for the first-excited vibronic state stem from a value of 2 and tend to a value just above 1.5 rather than to 1 and just above 0.5 for the ground vibronic states, reflecting the difference in zero-point energies.

V. SUMMARY

In this paper, we have discussed the case of the $E\otimes e$ JT system with linear and quadratic couplings and in the presence of additional symmetry-lowering distortions. We have

considered combinations of two different non-cubic distortions as all distortions are not equivalent when quadratic coupling is included. Often, previous papers have considered non-cubic distortions in the Q_θ direction only.[6]

Q_θ-type distortions enhance one of the minima formed by quadratic coupling but does not alter the position of the minimum. When Q_ϵ-type distortions are also included, the vibrational and pseudorotational dynamics become considerably more complicated. We have obtained analytical expressions for the quantum-mechanical ground state that clearly illustrates this dynamics. Our results agree well with those obtained from a Lanczos diagonalization method. Even better agreement could be obtained by including coupling to the upper APES, but this is not attempted here as the simplicity of the form of the wave functions would be lost.

For weak quadratic coupling, we find that the area of particular interest is the region of weak-to-intermediate linear coupling where the system reacts differently for the strong and weak strains. In contrast, in the regions of strong linear JT coupling, there is no observable dependence of the results on the value of the strain. An explanation for this is that the effective strength of the quadratic coupling is proportional not only to the quadratic coupling constant but also to the square of the linear coupling constant. When the effects of the quadratic coupling are strong, the motion of the system is localized around one of three deep wells in the APES. Strain has very little effect on these wells. Similarly, when there is a strong strain in a direction that coincides with one of the wells, the strength of the quadratic coupling has very little effect on the results because the quadratic coupling has little effect on the deep well generated by the strain.

The results in this paper help suggest the ranges of parameter values, for which it is a good approximation to neglect either the quadratic coupling or non-cubic distortions in any future studies. In addition, we have shown that much of the behavior of the system can be deduced by examining a simple algebraic expression for the effective potential. This is considerably simpler than performing a complete analysis of the wave functions and their energies.

The methods presented in this paper are applicable to systems of other symmetries such as the icosahedral JT problem that models the fullerene anions. These systems are considerably more complicated than the $E \otimes e$ system but similar ideas should apply. The model we have developed can be used as a starting point for the investigation of the cooperative JT effect in such systems.

*janette.dunn@nottingham.ac.uk

[1] H. A. Jahn and E. Teller, Proc. R. Soc. London, Ser. A **161**, 220 (1937).
[2] M. D. Kaplan and B. G. Vekhter, *Cooperative Phenomena in Jahn-Teller Crystals* (Plenum, New York, 1995).
[3] P. W. Stephens, L. Mihaly, P. L. Lee, R. L. Whetten, S. M. Huang, R. Kaner, F. Deiderich, and K. Holczer, Nature (London) **351**, 632 (1991).
[4] J. Geck, P. Wochner, S. Kiele, R. Klingeler, A. Revcolevschi, M. V. Zimmermann, B. Büchner, and P. Reutler, New J. Phys. **6**, 152 (2004).
[5] A. Sadoc, R. Broer, and C. DeGraaf, J. Chem. Phys. **126**, 134709 (2007).
[6] R. Englman and B. Halperin, Phys. Rev. B **2**, 75 (1970).
[7] O. Gunnarsson, Rev. Mod. Phys. **69**, 575 (1997).
[8] J. L. Martins, R. Car, and J. Buttet, J. Chem. Phys. **78**, 5646 (1983).
[9] J. Schön and H. Köppel, Chem. Phys. Lett. **231**, 55 (1994).
[10] P. García-Fernández, I. B. Bersuker, J. A. Aramburu, M. T. Barriuso, and M. Moreno, Phys. Rev. B **71**, 184117 (2005).
[11] Y. V. Yablokov, M. A. Augustyniak-Jablokow, M. Hitchman, and D. Reinen, Adv. Quantum Chem. **44**, 483 (2003).
[12] M. J. Riley, M. A. Hitchman, and A. W. Mohammed, J. Chem. Phys. **87**, 3766 (1987).
[13] I. B. Bersuker, *The Jahn-Teller Effect* (Cambridge University Press, Cambridge, 2006).
[14] H. C. Longuet-Higgins, U. Öpik, M. H. L. Pryce, and R. A. Sack, Proc. R. Soc. London, Ser. A **244**, 1 (1958).
[15] M. S. Child and H. C. Longuet-Higgins, Philos. Trans. R. Soc. London, Ser. A **254**, 259 (1961).
[16] C. C. Chancey, J. Phys. A **17**, 3183 (1984).
[17] I. B. Bersuker and V. Z. Polinger, *Vibronic Interactions in Molecules and Crystals* (Springer, Berlin, 1989).
[18] A. Thiel and H. Koppel, J. Chem. Phys. **110**, 9371 (1999).
[19] K. A. Bosnick, Chem. Phys. Lett. **317**, 524 (2000).
[20] J. L. Dunn and M. R. Eccles, Phys. Rev. B **64**, 195104 (2001).
[21] T. Sato, L. F. Chibotaru, and A. Ceulemans, J. Chem. Phys. **122**, 054104 (2005).
[22] S. N. Evangelou, M. C. M. O'Brien, and R. S. Perkins, J. Phys. C **13**, 4175 (1980).
[23] H. Koizumi and I. B. Bersuker, Phys. Rev. Lett. **83**, 3009 (1999).
[24] E. A. Moujaes, J. L. Dunn, and C. A. Bates, J. Mol. Struct. **838**, 238 (2007).
[25] I. Sioutis, V. L. Stakhursky, R. M. Pitzer, and T. A. Miller, J. Chem. Phys. **126**, 124308 (2007).
[26] M. J. Riley, M. A. Hitchman, and D. Reinen, Chem. Phys. **102**, 11 (1986).
[27] S. Murumatsu and N. Sakamoto, J. Phys. Soc. Jpn. **26**, 1273 (1979).
[28] M. C. M. O'Brien and S. N. Evangelou, J. Phys. C **13**, 6113 (1980).
[29] N. Manini, P. Gattari, and E. Tosatti, Phys. Rev. Lett. **91**, 196402 (2003).
[30] D. Ippolito, L. Martinelli, and G. Bevilacqua, Phys. Rev. B **71**, 064419 (2005).
[31] G. Bevilacqua, L. Martinelli, and G. P. Parravicini, Phys. Rev. B **54**, 7626 (1996).
[32] D. S. Scott, Oak Ridge National Laboratory Technical Report No. 84-08, 1979 (unpublished).
[33] E. A. Moujaes, Ph.D. thesis, University of Nottingham, 2007.